Hemispherically Aggregated $BaTiO_3$ Nanoparticle Composite Thin Film for High-Performance Flexible Piezoelectric Nanogenerator

Sung-Ho Shin,[†] Young-Hwan Kim,[†] Min Hyung Lee,[‡] Joo-Yun Jung,[§] and Junghyo Nah[†,*]

[†]Department of Electrical Engineering, Chungnam National University, Daejeon 305-764, Korea, [‡]Department of Applied Chemistry, Kyung Hee University, Yongin, Gyeonggi 446-701, Korea, and [§]Department of Nano Manufacturing Technology, Korea Institute of Machinery and Materials, Daejeon 305-343, Korea

ABSTRACT We report high-performance flexible nanogenerators (NGs) based on a composite thin film, composed of hemispherically aggregated $BaTiO_3$ nanoparticles (NPs) and poly(vinylidene fluoride-*co*-hexafluoropropene) P(VDF-HFP). The hemispherical BTO—P(VDF-HFP) clusters were realized by a solvent evaporation method, which greatly enhanced piezoelectric power generation. The flexible NGs exhibit high electrical output up to ~75 V and ~15 μA at the applied force normal to the surface, indicating the important role of hemispherical BTO clusters. Besides, the durability and reproducibility of the NGs were tested by cyclic measurement under bending stage, generating the output of ~5 V and ~750 nA. The approach we introduce here is simple, cost-effective, and well-suited for large-scale high-performance flexible NG fabrication.

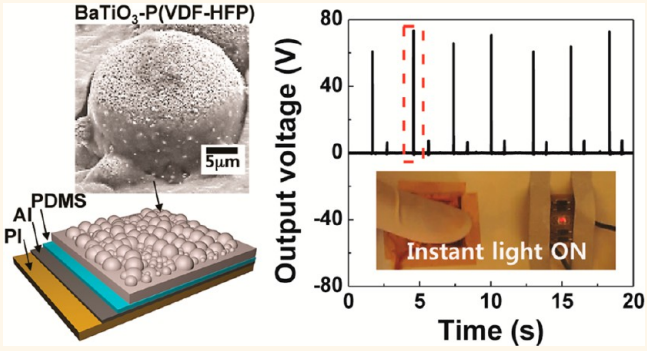

KEYWORDS: piezoelectric nanogenerator · $BaTiO_3$ nanoparticle · P(VDF-HFP) composite · flexible electronics

Power generation using fossil energy resources now faces critical issues as shortage and depletion of resources and pollution associated with their byproducts is expected to be exacerbated over the next decade.[1] To alleviate this trend, harvesting energy from various renewable energy resources has gained much attention.[2] More recently, in addition to conventional large-scale energy harvesting schemes, several small-scale energy harvesting methods, using solar,[3,4] thermal gradient,[5,6] and piezoelectric[7,8] or triboelectric effects,[9,10] have also been actively investigated to realize self-powering wireless electronic devices.[11−13] Among these approaches, piezoelectric power generation is considered as one of the most viable and promising routes as it is relatively less affected by external conditions.[14]

To date, piezoelectric materials, such as ZnO,[15,16] $PbZr_xTi_{1-x}O_3$ (PZT),[17,18] and $BaTiO_3$ (BTO),[19,20] have been widely examined to realize piezoelectric nanogenerators (NGs). Despite significant advances in ZnO NGs,[21,22] inherently low piezoelectric property limits further enhancement of device performances.[23] On the other hand, both PZT and BTO have a perovskite crystal structure with very high piezoelectric constant.[24−26] Thus, the NGs fabricated with these materials are expected to greatly improve output power generation. Recently, the performance of the BTO NGs, more environmentally safe by comparison to PZT, was reported, where the NGs were fabricated by compositing BTO nanoparticles (NPs) with poly(dimethylsiloxane) (PDMS).[27,28] The key aspect for high output power generation in the reports was on how to uniformly distribute BTO NPs in the composite. Since BTO NPs in the polymer composite are naturally subsided to the bottom of the layer, it was essential to supplement filling materials as carbon nanotubes[27] and virus template[28] in the composite to promote distribution of BTO NPs throughout the polymer layer. In light of this issue, it is necessary to further investigate the novel and

* Address correspondence to jnah@cnu.ac.kr.

Received for review December 18, 2013 and accepted February 11, 2014.

Published online February 11, 2014
10.1021/nn406481k

© 2014 American Chemical Society

facile ways to attain BTO NP composite thin film for the realization of high-performance NGs.

Herein, we report high-performance flexible NGs based on the composite thin film, composed of hemispherically aggregated BTO NP−P(VDF-HFP). The composite thin film was prepared by solvent evaporation of the spin-coated solution, containing BTO NPs with the tetragonal phase, P(VDF-HFP), dimethylformamide (DMF), and acetone. The aggregated BTO−P(VDF-HFP) cluster formation improves piezoelectric power generation by boosting total dipole moment inside the cluster and providing an effective structure for mechanical stress harvesting. Our NGs demonstrate open-circuit voltage of ∼75 V and short-circuit current of ∼15 μA at the applied pressure of ∼0.23 MPa, generating enough power to instantly turn on a commercial red-light-emitting diode (LED). Besides, the NGs showed durability and reproducibility under periodic bending cycles. The approach we introduce here is simple, cost-effective, and well-suited for large-scale high-performance flexible NG fabrication.

RESULTS AND DISCUSSION

Figure 1a shows the schematic representation of the device fabrication process. First, a Si wafer piece is cleaned with acetone, IPA, deionized (DI) water, and N_2, respectively (Figure 1a). Next, using the BTO NPs (U.S. Research Nanomaterials, Inc.), the solution is prepared by mixing with P(VDF-HFP), BTO NPs, DMF, and acetone. The detailed solution preparation process is described in the Experimental Method section. The BTO NPs have an average size of 200 nm (Figure 1i), where the Raman spectrum in Figure 1i (inset) reveals that the BTO NPs have a tetragonal phase, exhibiting a high piezoelectric coefficient.[29] The peaks of the Raman spectrum are positioned at 256 cm^{-1} [A_1(TO)], 306 cm^{-1} [E, B_1(TO+LO)], 513 cm^{-1} [E, A_1(TO)], and 715 cm^{-1} [E, A_1(LO)], all of which are subjective to a tetragonal phase of BTO.[30,31] The prepared solution is then spin-coated on the precleaned Si substrate and cured in an oven at 80 °C for 1 h under ambient conditions (Figure 1b). During the curing process, hemispherical BTO clusters are formed as the solvents (acetone and DMF) are evaporated. Figure 1g shows a scanning electron micrograph (SEM) of BTO−P(VDF-HFP) composite hemispheres. The diameter of the hemisphere is varied from a few micrometers to ∼50 μm. Next, the composite thin film with BTO clusters is peeled off from the Si substrate (Figure 1c). We note that the composite thin film can be easily detached from the substrate. Lastly, the top and bottom sides of the composite thin film are encapsulated with coated PDMS-coated metal electrodes (Al) on polyimide (PI) films before the spin-coated PDMS is cured (Figure 1d,e). The spin-coated PDMS on Al/PI will first fill the gaps between BTO clusters and completely cover the hemispheres.

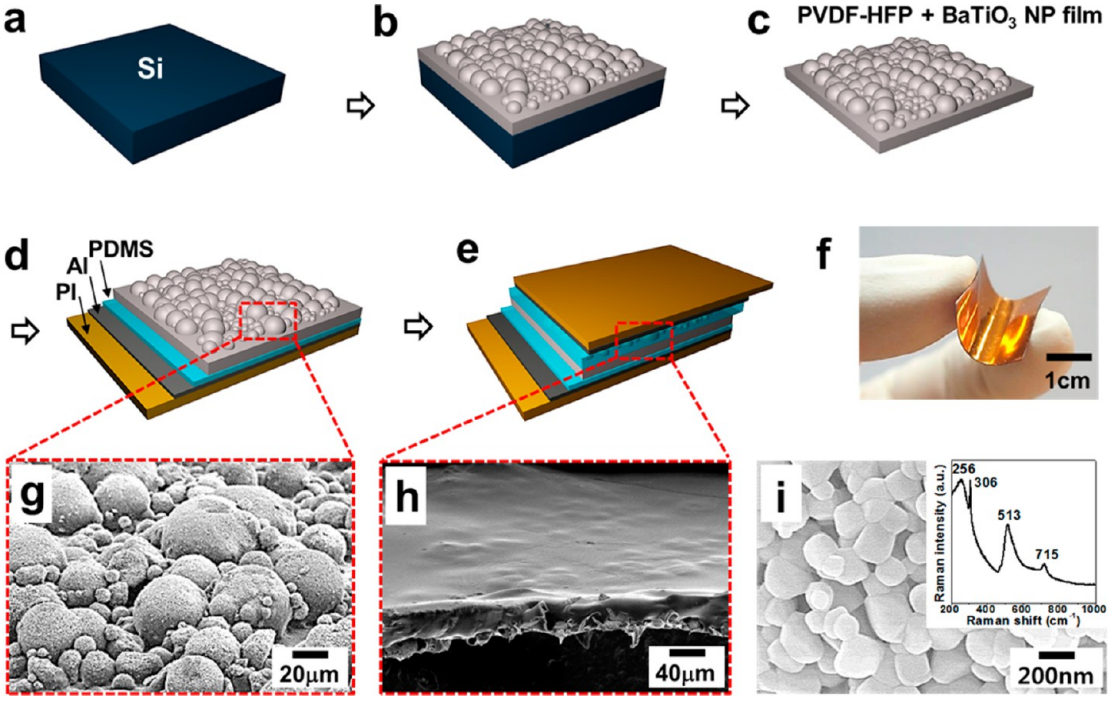

Figure 1. (a−e) Schematic diagram of the NG fabrication process. (a) Silicon substrate. (b) BTO−P(VDFP-HFP) composite thin film cured after solvent evaporation of spin-coated solution. (c) Peeled off composite thin film from the Si substrate, followed by high electric field poling process. (d) PDMS-coated Al/PI electrode layer attachment on a bottom side. (e) PDMS spin-coating on BTO−P(VDF-HFP) composite film, followed by attachement of top electrode. (f) Photograh of the fabricated NG at bent state, exhibiting flexibility of the device. (g) SEM image of the BTO−P(VDF-HFP) composite film consisted of BTO clusters. (h) SEM of the PDMS-covered BTO−P(VDF-HFP) layer. (i) SEM image of the BTO NPs. The inset displays a Raman spectrum observed from the BTO NPs.

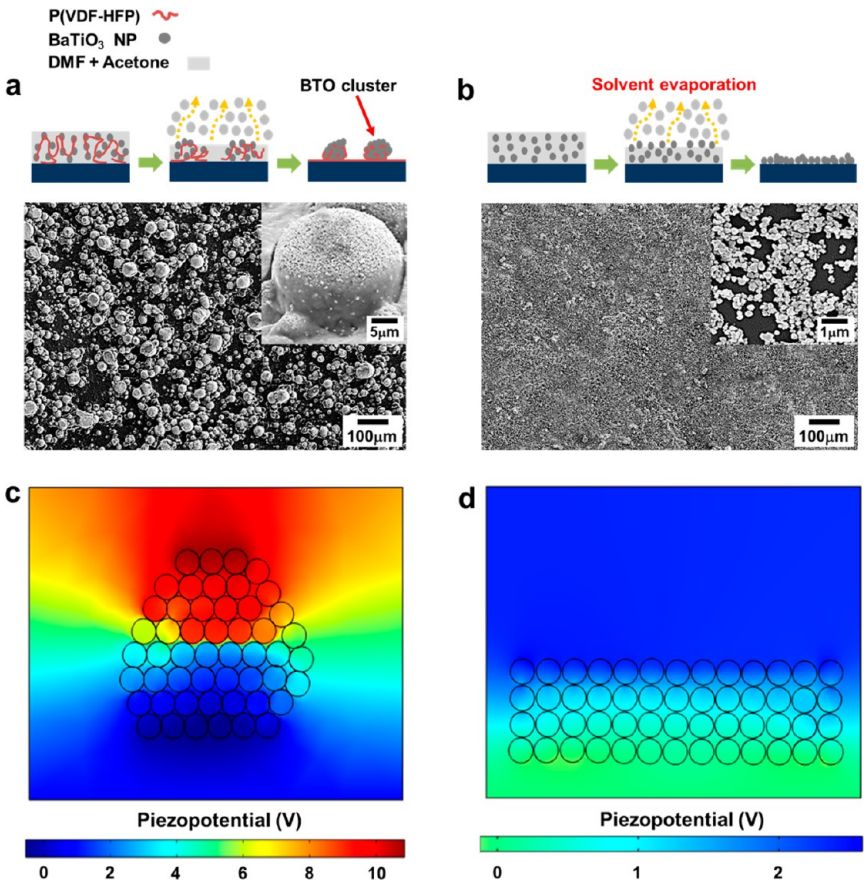

Figure 2. (a) Schematic flow and a top view SEM of BTO−P(VDF-HFP) clusters, where BTO NPs are hemispherically aggregated to form clusters. The inset is a magnified SEM of a BTO cluster. (b) Schematic flow and a top view SEM of BTO NP layer, formed by dispersing the solution without P(VDF-HFP). The BTO NPs are stacked laterally onto the substrate. (c) Simulation result of the piezopotential distribution in a hemisphercally aggregated BTO cluster. (d) Simulation of the piezopotential distribution in the stacked BTO NPs at the bottom region. Note: the same number of BTO NPs were used in both results. The simulation explicitly shows the importance of BTO NP distribution for the output performance.

The SEM image of the compactly packed BTO NP clusters is shown in Figure 1h, where the rough surface indicates the regions where BTO clusters are covered with PDMS. The solvent-evaporation-assisted solution coating method used in this study is simple, cost-effective, and suitable for large-scale production. Figure 1f shows an optical image of the fabricated flexible NG.

Figure 2 explains the formation of the BTO hemisphere and its effect on piezoelectric potential generation. The schematic drawings in Figure 2a illustrate the role of P(VDF-HFP) on the formation of BTO NP hemispheres. The P(VDF-HFP) copolymer (Sigma-Aldrich) works here as polymer linkage forming BTO hemispheres as demonstrated in Figure 2a. As the solvents (DMF, acetone) in the spin-coated solution are rapidly evaporated in the oven at 80 °C, the remaining P(VDF-HFP) and BTO NPs are aggregated into the composite hemispheres. In Figure 2a, the BTO NP hemispheres with large diameters can be clearly observed. Besides, it is noticeable that BTO hemispheres are not completely covered with a thick P(VDF-HFP) (Figure 2a, inset). We note here that the mixing ratio between solvents, P(VDF-HFP), and BTO NPs in the solution was carefully determined to avoid BTO hemispheres being completely covered with the P(VDF-HFP). Due to relatively high Young's modulus of P(VDF-HFP),[32] once the BTO hemispheres are completely covered with a thick P(VDF-HFP) layer, it can be detrimental to the performance of the piezoelectric NGs. The detailed composite ratio of the solution is described in the Experimental Method section. To distinctly show the role of P(VDF-HFP) copolymer, the composite solution, not containing P(VDF-HFP), was examined, as well. In the absence of P(VDF-HFP), the aggregation of the BTO NPs was significantly reduced in comparison to BTO hemispheres (Figure 2b). Next, to qualitatively understand the roles of the BTO hemisphere formation on the performance of the NGs, we examined the generated piezoelectric potentials at the applied compressive force normal to the surface. Using COMSOL simulation software, the piezoelectric potentials were generated for two different BTO NP distribution patterns, one as a hemispherical cluster (Figure 2c) and the other as planar distribution at the bottom (Figure 2d). For a fair comparison, the same number of BTO

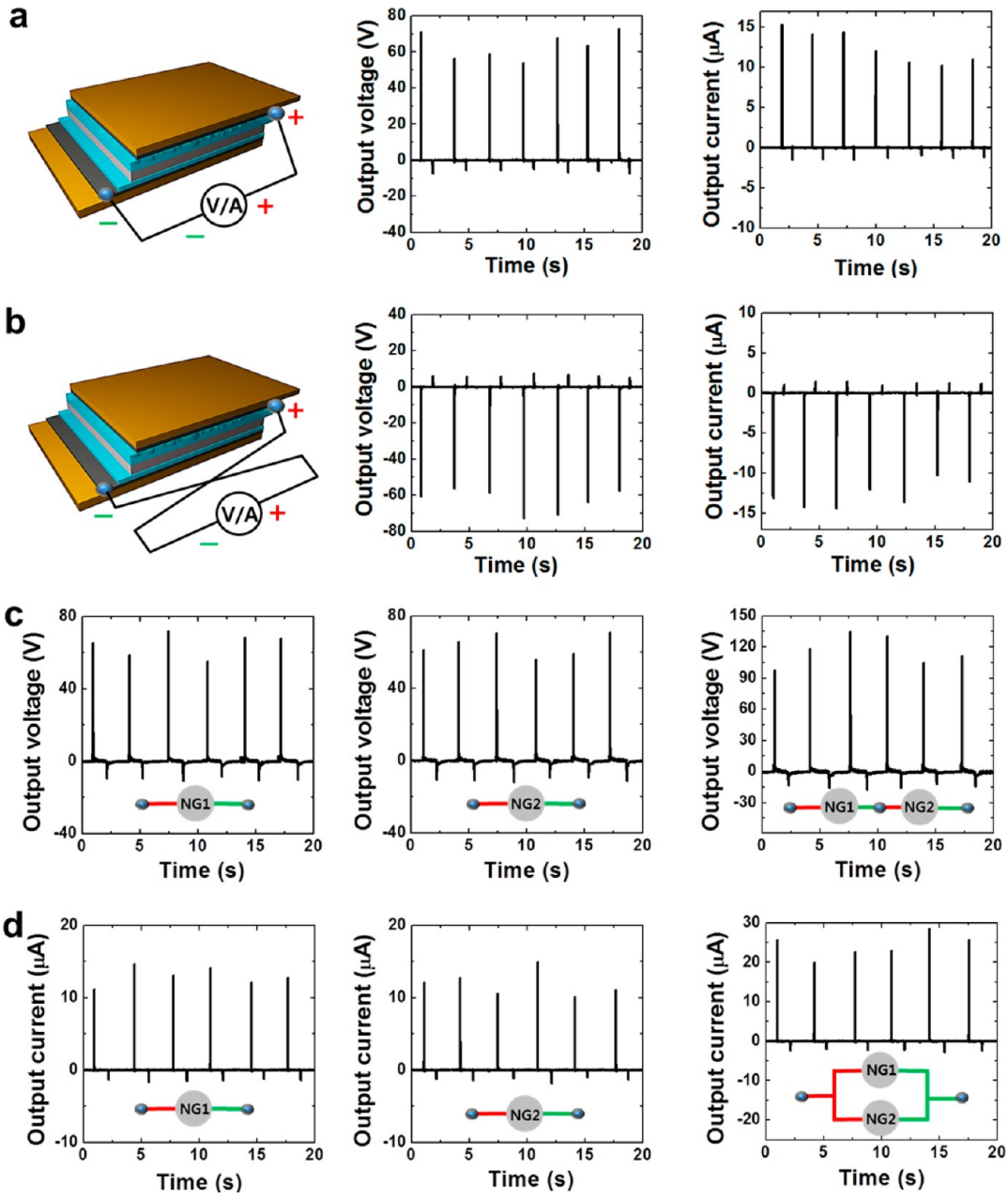

Figure 3. Output performance (open-circuit voltage and short-circuit current) of the NGs. (a,b) Switching polarity test. (a) Measured output voltage and current under the forward connection mode. (b) Output voltage and current under the reverse connection mode. (c,d) Linear superposition measurement. (c) Under the serial connection mode of two NGs, the output voltage reaches 2-fold higher value by comparison to the one in a single NG. (d) In the parallel connection mode of two NGs, the current is doubled in comparison to a single NG.

particles was included in the both simulations, nestled in the PDMS layer. The generated piezoelectric output voltages at the same compressive force, 0.23 MPa, are ~8.5 V for the NG with hemispherical BTO NP formation and ~2.1 V for the one with laterally distributed BTO NPs. The obvious piezoelectric potential increase clearly indicates the role of BTO cluster formation. When BTO NPs form hemispherical clusters, total dipole moment inside the cluster increases in proportion to the diameter of the BTO hemisphere. Besides, hemispherical BTO clusters provide more effective structure for harvesting externally applied stresses, as well. On the other hand, considerably weak piezoelectric potential is obtained when BTO distribution is localized near the bottom surface. We also note that the height of BTO clusters in the actual NGs demonstrated in this work is much greater by comparison to that of BTO NPs dispersed without including P(VDF-HFP). Hence, the potential difference is expected to be greater than the simulation results.

Using the BTO–P(VDF-HFP) thin film as an active layer, the piezoelectric NGs were fabricated and characterized (Figure 3). The area of device measured here was 4 cm^2, and its active area under pressure was

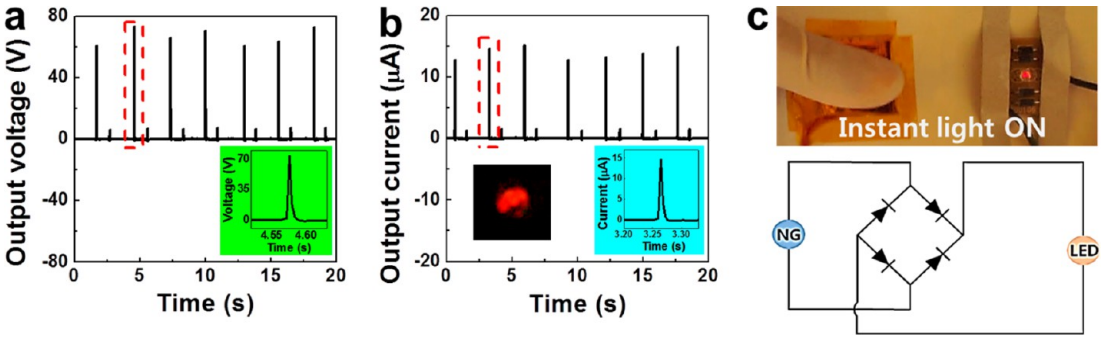

Figure 4. Rectified output signals of a NG and a commercial LED driving with its output. (a) Rectified open-circuit voltages of the NG with a full wave rectifier under periodic finger impact. The inset is an enlarged view of a voltage pulse in the dashed line. (b) Rectified currents of the NG under periodic finger impact. (Inset) LED lighting. (c) Instant LED light on upon a finger impact and a bridge rectifier circuit diagram.

~2.2 cm^2. Under periodically applied pressure of ~0.23 MPa, measured using the load cell (Bongshin, Inc.), the maximum output voltage and current up to ~75 V and ~15 μA were obtained, respectively. This result is one of the highest output power generations in the piezoelectric NGs reported to date. In comparison, the performance of the NG only with BTO NPs was also measured in Figure S1, where the NPs are subsided in PDMS as in Figure 2d, and approximately an order of magnitude lower output performance can be clearly noticed. Here, we note that all BTO thin films were poled under high electric field (100 kV/cm). Unless the BTO thin film is poled under high electric field, considerably low output signals are obtained as in Figure S2. The poling process aligns randomly oriented dipoles in the BTO NPs, which is an essential step for enhancing the output performance of the NGs. In our BTO−P(VDF-HFP) thin film NGs, even if the measured output signals are mainly from BTO clusters, it is still necessary to verify contribution of P(VDF-HFP), which is also a piezoelectric material but with a low piezoelectric coefficient.[33] Thus, we fabricated the NGs only with a P(VDF-HFP) layer by excluding BTO NPs in the solution. After a high voltage poling process, P(VDF-HFP) film was characterized by Fourier transform infrared spectroscopy (FTIR), where it shows α-phase properties, exhibiting negligible piezoelectric properties[34] (Figure S3a). Consequently, negligible output voltage and current were observed in the NGs (Figure S3b,c). These results confirmed that the generated output signals were dominantly from BTO clusters. We note here that the role of P(VDF-HFP) is limited to hemispherically aggregate BTO NPs. Due to its low viscosity and high solubility in the solvents, BTO NPs can be easily mixed and well-distributed in the solution. In addition, prompt thin film formation can be easily achieved by rapid solvent evaporation from the spin-coated solution, which is essential to form hemispherical BTO clusters.

The current and voltage generation mechanism of the NG can be described by transient charge flows, induced by piezoelectric potential of dipole moments in BTO between two electrodes. When a compressive force is applied to the NG, the piezoelectric potential created in the BTO cluster leads charges to flow through an external circuit between top and bottom electrodes, until it is balanced by these charges. As the applied force is released, the charges flow back to balance the potential difference between two electrodes. The notable output performance in Figure 3a is due to hemispherical aggregation of BTO NPs, as indicated in Figure 2c. In addition, the PDMS packing layer also contributes to enhance the output performance. The spin-coated PDMS solution fills the gap between BTO NPs in the hemispherical clusters. Thus, when a force applied from any direction, the stress can be more effectively transferred to entire BTO NPs in the clusters, resulting in the enhancement of the NG's performance, providing similar advantages reported previously.[35] Next, to confirm the validity of the output signals, the NGs were measured under different connection modes.[36,37] First, the NG was measured under a reverse connection for the switching polarity test (Figure 3b). The amplitudes of the output signals under a reverse connection were almost the same as the ones under a forward connection, while the polarity of the signal was reversed (supplementary video file 1). Second, the linear superposition measurement was conducted with the two NGs. The generated output signals under the serial and parallel connection mode are displayed in Figure 3c,d, respectively. When the NGs are under a serial connection, the maximum voltage, ~134 V, can be obtained (Figure 3c). While under a parallel connection, the maximum current, ~28 μA, can be generated (Figure 3d). The linear superposition demonstrates that targeting either output voltage or current can be achieved by integrating NGs in serial or parallel connections. These results also confirm that the measured output signals are indeed from the NGs.

To prove a practical application of the NG, we connected a NG to a commercial light-emitting diode through a bridge rectifier consisting of four diodes (Figure 4c), which convert the generated AC to DC

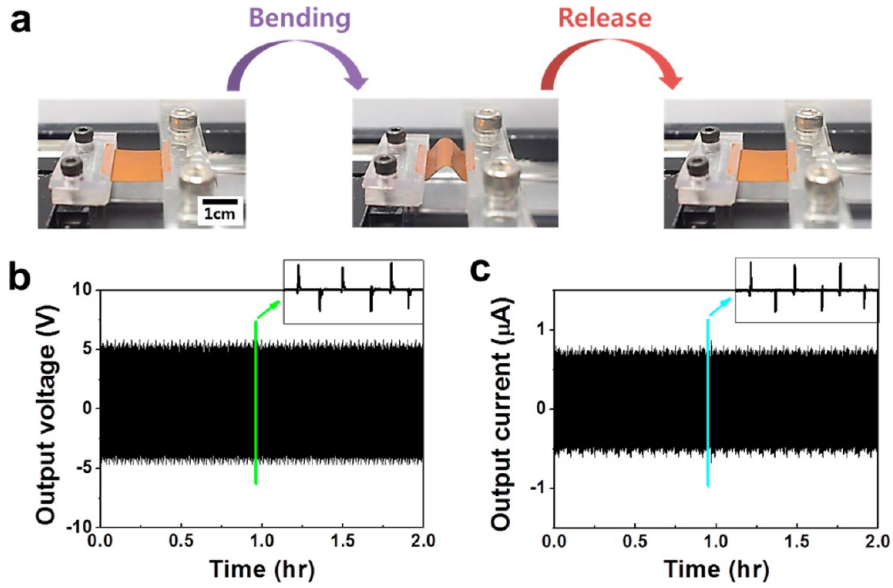

Figure 5. (a) Optical images of the NG at bending and releasing state on the bending stage. (b) Cyclic measurement of open-circuit voltages for 5400 cycles. The inset displays magnified signals with the green dashed line. (c) Cyclic measurement of short-circuit current for 5400 cycles. The inset shows magnified signals with the sky-blue dashed line.

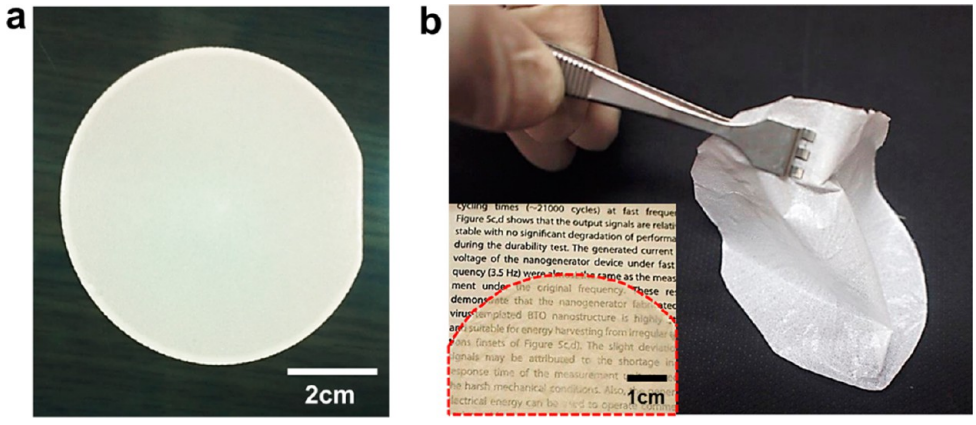

Figure 6. Optical images of the BTO–P(VDF) composite thin film processed for large-scale demonstration. (a) Photograph of a BTO–P(VDF-HFP) composite film on a 3 in. wafer using a simple solution coating method. (b) Photograph of a BTO–P(VDF-HFP) composite thin film, peeled off from a 3 in. wafer. The image reveals that the composite film is ultraflexible. (Inset) Composite thin film looks semitransparent due to its thickness.

signals. The rectified output voltage and current are displayed in Figure 4a,b, respectively. It can be noticed that a commercial LED with operation voltage of 2 V is directly connected with the developed NG without the aid of a capacitor (Figure 4c). The NG was triggered by a finger push, and it instantly turns the red LED on as in Figure 4b (inset) (supplementary video file 2).

In Figure 5, reproducibility and reliability of the NGs were also examined by bending the devices using a bending stage for sufficient bending cycles. The NG was bent and released repeatedly for 2 h, where consistent output voltage and current were generated and maintained over 5400 bending cycles (Figure 5b,c). We conducted these measurements for multiple devices and confirmed similar output performances. In addition, performance degradation was not observed even if the device measured again after a couple of weeks. These results distinctly show that our NG satisfies both criteria. Lastly, to show suitability of our method for large-scale NG fabrication, we presented the BTO–P(VDF-HFP) composite layer formation on a 3 in. wafer (Figure 6a). Figure 6b reveals that the active NG layer is very flexible and thin. Therefore, our approach can be effectively expanded to fabricate high-performance NGs in large scale by a simple, fast, and cost-effective process.

CONCLUSION

In summary, we have demonstrated a novel approach for realizing high-performance flexible piezoelectric NGs based on BTO–P(VDF-HFP) composite thin film. The formation of hemispherical BTO NP clusters by

solvent evaporation method has enabled us to achieve improved piezoelectric output power generation. In addition, this cluster formation offers effective structure for harvesting externally applied mechanical stress, as well. Consequently, the NGs generate much enhanced output power, instantly lighting up a commercial LED. By cyclic bending test using a bending stage, superb reproducibility and durability of the NGs were also confirmed. The approach we proposed here is suitable for large-scale high-performance flexible NG fabrication. Furthermore, due to ultrathin and flexible nature of active composite layer, it can be potentially adopted as a promising flexible power supply for realizing self-powered electronics.

EXPERIMENTAL METHOD

BTO NP−P(VDF-HFP) Composite Solution. A total of 0.75 g of P(VDFP-HFP) (Sigma-Aldrich) was dissolved in a mixture of 1.5 mL of DMF and 4.5 mL of acetone. The solution was then heated at 60 °C for 40 min in the encapsulated container and cooled for 30 min in an ambient condition. Next, 30 wt % of BTO NPs was mixed with the prepared solution and stirred for 2 h on a magnetic stirring plate.

Nanogenerator Fabrication. The BTO−P(VDF-HFP) composite solution was spin-coated at 2000 rpm for 30 s on a Si wafer piece and cured in an oven at 80 °C for 1 h. The cured composite thin film with BTO clusters was peeled off from the Si substrate. The 100 nm thick Al was evaporated on two flexible substrates (PI, 50 and 200 μm thick) as top and bottom electrodes. The PDMS (Sylgard, 184 SILICONE ELASTOMER) was then spin-coated on the Al-deposited backside electrode at 5000 rpm for 40 s and precured in an oven at 80 °C for 5 min. Next, the backside of the BTO−P(VDF-HFP) composite thin film was attached to the precured PDMS-coated polyimide substrate and cured in an oven at 80 °C for 1 h. The PDMS solution was again spin-coated (4500 rpm for 30 s) on the BTO−P(VDF-HFP)/PDMS/Al-deposited PI, followed by precuring in an oven at 80 °C for 5 min. The topside electrode was covered on the precured structure, cured in an oven at 80 °C for 2 h, and kept in ambient condition for a day. Lastly, the fabricated device was poled at 100 °C while applying a direct electric field of 100 kV/cm for 20 h.

Electrical Measurement. The output voltage and current from the NGs were measured by using a voltage meter (Agilent, 34401A) and current preamplifier (Stanford Research Systems, SR 570), respectively. By using a bending stage, the cyclic measurement of NGs was performed. The compressive force normal to the NG's surface was measured by a load cell (Bongshin, Inc.).

Characterization. A FTIR spectrometer (Bio-Rad Laborartories, Inc., FTS-175C) was used to analyze the phase type of P(VDF-HFP) film. Tetragonal phase of BTO NPs was confirmed by a high-resolution Raman spectrometer.

Conflict of Interest: The authors declare no competing financial interest.

Acknowledgment. This research was supported by Basic Science Research Program through the National Research Foundation of Korea (NRF-2012R1A1A1041869).

Supporting Information Available: Additional figures include the performance of BTO-only NG, the NG without high voltage poling process, P(VDF-HFP)-only NG, *etc*. The additional movie files include the NG under forward/reverse connection modes and instant lighting up of a red LED by finger push. This material is available free of charge *via* the Internet at http://pubs.acs.org.

REFERENCES AND NOTES

1. Hudson, M. The Final Energy Crisis. *Environ. Pollut.* **2006**, *15*, 677–679.
2. Wang, Z. L.; Wu, W. Nanotechnology-Enabled Energy Harvesting for Self-Powered Micro-/Nanosystems. *Angew. Chem., Int. Ed.* **2012**, *51*, 2–24.
3. Shin, J. C.; Mohseni, P. K.; Yu, K. J.; Tomasulo, S.; Montgomery, K. H.; Lee, M. L.; Rogers, J. A.; Li, X. Heterogeneous Integration of InGaAs Nanowires on the Rear Surface of Si Solar Cells for Efficiency Enhancement. *ACS Nano* **2012**, *6*, 11074–11079.
4. Yang, J.; You, J.; Chen, C.-C.; Hsu, W.-C.; Tan, H.-R.; Zhang, X. W.; Hong, Z.; Yang, Y. Plasmonic Polymer Tandem Solar Cell. *ACS Nano* **2011**, *5*, 6210–6217.
5. Yang, Y.; Guo, W.; Pradel, K. C.; Zhu, G.; Zhou, Y.; Zhang, Y.; Hu, Y.; Lin, L.; Wang, Z. L. Pyroelectric Nanogenerators for Harvesting Thermoelectric Energy. *Nano Lett.* **2012**, *12*, 2833–2838.
6. Yang, Y.; Wang, S.; Zhang, Y.; Wang, Z. L. Pyroelectric Nanogenerators for Driving Wireless Sensors. *Nano Lett.* **2012**, *12*, 6408–6413.
7. Xu, S.; Yeh, Y.-W.; Poirier, G.; McAlpine, M. C.; Register, R. A.; Yao, N. Flexible Piezoelectric PMN−PT Nanowire-Based Nanocomposite and Device. *Nano Lett.* **2013**, *13*, 2393–2398.
8. Chang, C.; Tran, V. H.; Wang, J.; Fuh, Y.-K.; Lin, L. Direct-Write Piezoelectric Polymeric Nanogenerator with High Energy Conversion Efficiency. *Nano Lett.* **2010**, *10*, 726–731.
9. Hu, Y.; Yang, J.; Jing, Q.; Niu, S.; Wu, W.; Wang, Z. L. Triboelectric Nanogenerator Built on Suspended 3D Spiral Structure as Vibration and Positioning Sensor and Wave Energy Harvester. *ACS Nano* **2013**, *7*, 10424–10432.
10. Lin, Z.-H.; Xie, Y.; Yang, Y.; Wang, S.; Zhu, G.; Wang, Z. L. Enhanced Triboelectric Nanogenerators and Triboelectric Nanosensor Using Chemically Modified TiO_2 Nanomaterials. *ACS Nano* **2013**, *7*, 4554–4560.
11. Hu, Y.; Zhang, Y.; Xu, C.; Lin, L.; Snyder, R. L.; Wang, Z. L. Self-Powered System with Wireless Data Transmission. *Nano Lett.* **2011**, *11*, 2572–2577.
12. Wang, Z. L. Self-Powered Nanosensors and Nanosystems. *Adv. Mater.* **2012**, *24*, 280–285.
13. Wang, Z. L. Toward Self-Powered Sensor Networks. *Nano Today* **2010**, *5*, 512–514.
14. Wang, Z. L.; Wang, X. D.; Song, J. H.; Liu, J.; Gao, Y. F. Piezoelectric Nanogenerators for Self-Powered Nanodevices. *IEEE Pervasive Computing* **2008**, *7*, 49–55.
15. Wang, Z. L.; Song, J. H. Piezoelectric Nanogenerators Based on Zinc Oxide Nanowire Arrays. *Science* **2006**, *312*, 242–246.
16. Yu, H. K.; Baik, J. M.; Lee, J.-L. Self-Connected and Habitually Tilted Piezoelectric Nanorod Array. *ACS Nano* **2011**, *5*, 8828–8833.
17. Chen, X.; Xu, S.; Yao, N.; Shi, Y. 1.6 V Nanogenerator for Mechanical Energy Harvesting Using PZT Nanofibers. *Nano Lett.* **2010**, *10*, 2133–2137.
18. Wu, W.; Bai, S.; Yuan, M.; Qin, Y.; Wang, Z. L.; Jing, T. Lead Zirconate Titanate Nanowire Textile Nanogenerator for Wearable Energy-Harvesting and Self-Powered Devices. *Nano Lett.* **2012**, *12*, 6231–6235.
19. Park, K.-I.; Xu, S.; Liu, Y.; Hwang, G.-T.; Kang, S.-J. L.; Wang, Z. L.; Lee, K. J. Piezoelectric $BaTiO_3$ Thin Film Nanogenerator on Plastic Substrates. *Nano Lett.* **2010**, *10*, 4939–4943.
20. Ni, X.; Wang, F.; Lin, A.; Xu, Q.; Yang, Z.; Qin, Y. Flexible Nanogenerator Based on Single $BaTiO_3$ Nanowire. *Sci. Adv. Mater.* **2013**, *5*, 1781–1787.
21. Lee, K. Y.; Kumar, B.; Seo, J.-S.; Kim, K.-H.; Sohn, J. I.; Cha, S. N.; Choi, D.; Wang, Z. L.; Kim, S.-W. P-Type Polymer-Hybridized High-Performance Piezoelectric Nanogenerators. *Nano Lett.* **2012**, *12*, 1959–1964.
22. Shin, S.-H.; Lee, M. H.; Jung, J.-Y.; Seol, J. H.; Nah, J. Piezoelectric Performance Enhancement of ZnO Flexible

Nanogenerator by a CuO−ZnO P−N Junction Formation. *J. Mater. Chem. C* **2013**, *1*, 8103–8107.
23. Karanth, D.; Fu, H. Large Electromechanical Response in ZnO and Its Microscopic Origin. *Phys. Rev. B* **2005**, *72*, 064116.
24. Luo, Y.; Szafraniak, I.; Zakharov, N. D.; Nagarajan, V.; Steinhart, M.; Wehrspohn, R. B.; Wendorff, J. H.; Ramesh, R.; Alexe, M. Nanoshell Tubes of Ferroelectric Lead Zirconate Titanate and Barium Titanate. *Appl. Phys. Lett.* **2003**, *83*, 440–442.
25. Scott, J. F. Applications of Modern Ferroelectrics. *Science* **2007**, *315*, 954–959.
26. Saito, Y.; Takao, H.; Tani, T.; Nonoyama, T.; Takatori, K.; Homma, T.; Nagaya, T.; Nakamura, M. Lead-Free Piezoceramics. *Nature* **2004**, *432*, 84–87.
27. Park, K.-I.; Lee, M.; Liu, Y.; Moon, S.; Hwang, G.-T.; Zhu, G.; Kim, J. E.; Kim, S. O.; Kim, D. K.; Wang, Z. L.; *et al.* Flexible Nanocomposite Generator Made of $BaTiO_3$ Nanoparticles and Graphitic Carbons. *Adv. Mater.* **2012**, *24*, 2999–3004.
28. Jeong, C. K.; Kim, I.; Park, K.-I.; Oh, M. H.; Paik, H.; Hwang, G.-T.; No, K.; Nam, Y. S.; Lee, K. J. Virus-Directed Design of a Flexible $BaTiO_3$ Nanogenerator. *ACS Nano* **2013**, *7*, 11016–11025.
29. Berlincourt, D.; Jaffe, H. Elastic and Piezoelectric Coefficients of Single-Crystal Barium Titanate. *Phys. Rev.* **1958**, *111*, 143–148.
30. Lee, H.-W.; Moon, S.; Choi, C.-H.; Kim, D. K. Synthesis and Size Control of Tetragonal Barium Titanate Nanopowders by Facile Solvothermal Method. *J. Am. Ceram. Soc.* **2012**, *95*, 2429–2434.
31. Li, A. D.; Ge, C. Z.; Lu, P.; Wu, D.; Xiong, S. B.; Ming, N. B. Fabrication and Electrical Properties of Sol−Gel Derived $BaTiO_3$ Films with Metallic $LaNiO_3$ Electrode. *Appl. Phys. Lett.* **1997**, *70*, 1616–1618.
32. Zhou, X.; Zhao, X.; Suo, Z.; Zou, C.; Runt, J.; Liu, S.; Zhang, S.; Zhang, Q. M. Electrical Breakdown and Ultrahigh Electrical Energy Density in Polyinylidene Fluoride-Hexafluoropropylene Copolymer. *Appl. Phys. Lett.* **2009**, *94*, 162901.
33. Malmonge, L. F.; Malmonge, J. A.; Sakamoto, W. K. Study of Pyroelectric Activity of PZT/PVDF-HFP Composite. *Mater. Res.* **2003**, *6*, 469–473.
34. He, X.; Yao, K.; Gan, B. K. Phase Transition and Properties of a Ferroelectric Poly(vinylidene fluoride-hexafluoropropylene) Copolymer. *J. Appl. Phys.* **2005**, *97*, 084101.
35. Zhu, G.; Wang, A. C.; Liu, Y.; Zhou, Y.; Wang, Z. L. Functional Electrical Stimulation by Nanogenerator with 58 V Output Voltage. *Nano Lett.* **2012**, *12*, 3086–3090.
36. Yang, R.; Qin, Y.; Dai, L.; Wang, Z. L. Power Generation with Laterally Packaged Piezoelectric Fine Wires. *Nat. Nanotechnol.* **2009**, *4*, 34–39.
37. Yang, R.; Qin, Y.; Li, C.; Dai, L.; Wang, Z. L. Characteristics of Output Voltage and Current of Integrated Nanogenerators. *Appl. Phys. Lett.* **2009**, *94*, 022905.